JOURNAL OF MECHANICAL ENGINEERING AND SCIENCES
ISSN: 2289-4659 e-ISSN: 2231-8380
VOLUME 19, ISSUE 2, 2025, 10667 - 10675
DOI: https://doi.org/10.15282/jmes.19.2.2025.8.0836

RESEARCH ARTICLE

Effect of divergent angle and water flowrate on mean bubble size in venturi-type generator: An experimental and computational approach

N. Nadumaran[1], E. A. Alias[1]*, M. H. Hamidi[1] , N. H. Johari[1,2]

[1] Faculty of Mechanical and Automotive Engineering Technology, Universiti Malaysia Pahang Al-Sultan Abdullah, 26600 Pekan, Pahang, Malaysia
[2] Centre for Advanced Industrial Technology, Universiti Malaysia Pahang Al-Sultan Abdullah, 26600 Pekan, Pahang, Malaysia
Phone: +6094315000: Fax.: +6094315555

ABSTRACT - Venturi nozzles, valued for their simple design and flexibility, are widely used to generate microbubbles (MB) via hydrodynamic cavitation, particularly in water treatment and agriculture. MB efficiency depends on bubble size, which is influenced by the Venturi geometry and flow parameters, such as divergent angle and water flow rate. However, the relationship between these factors and bubble size remains underexplored, especially through combined experimental and simulation approaches. This study addresses that gap by combining experimental visualization and computational fluid dynamics to assess the impact of divergent angle and water flow rate on MB generation. Three Venturi nozzles with divergent angles of 8°, 10°, and 12°, and flow rates of 13 L/min, 33 L/min, and 66 L/min were tested. Bubble size was measured using high-speed imaging and analyzed in MATLAB. Simulations were performed using ANSYS FLUENT with a coupled Eulerian–Lagrangian model and a Population Balance Model, enabling the detailed prediction of bubble size. Experimental and simulation results showed a relative error of less than 5%, confirming the reliability of simulations. Increasing the divergent angle and flow rate decreased the MB distribution, yielding smaller bubbles. The Venturi 3 (12° divergent angle) produced the smallest bubbles, measured experimentally at 519 µm and in simulations at 505 µm, at a flow rate of 66 L/min. The strong agreement between experimental and simulation results, with a maximum error of 4%, was supported by velocity profile analysis, which revealed the highest velocity (14.09 m/s) in Venturi 3, resulting in the formation of the smallest bubbles. These findings not only validate the effectiveness of the simulations in predicting bubble size but also offer valuable insights for optimising venturi designs.

ARTICLE HISTORY
Received : 28th Nov. 2024
Revised : 02nd May 2025
Accepted : 09th June 2025
Published : 30th June 2025

KEYWORDS
Microbubble
Bubble size
Divergent angle
Water flowrate

1. INTRODUCTION

Microbubbles, also known as MBs, are small, gas-filled bubbles with distinct properties, including excellent solubility, slow rise velocity, high dissolution rate, self-compression effect, surface adsorption, and acoustic properties [1-4]. These characteristics have made MBs beneficial for various purposes in fields such as water treatment [5], agriculture [5], aquaculture [6], and the food industry [7]. Researchers have developed various MB generators, including pressurised dissolution, spiral liquid flow, porous plates, and venturi nozzles, to produce MBs efficiently [8]. Among these generators, Venturi nozzles are frequently used to produce MBs due to their cost-effectiveness and low energy consumption [9]. A Venturi's performance is commonly evaluated based on the size and density of the produced MBs, which are tailored to specific application requirements [10]. As a result, numerous studies have been conducted to investigate the impact of geometrical configuration and flow condition variations on the generated bubble size, to control the size distribution.

Research indicates that the divergent angle and water flow rate are primary factors influencing the mechanism of bubble formation, which subsequently affects the generated size distribution [11-13]. Significant investigations into geometrical and flow parameters have been conducted through experimental or simulation studies [13, 16-19]. Zhao et al. [17] performed an experimental study using a high-speed camera to investigate the influence of divergent angles on bubble movement and breakup in venturi channels. Three venturi channels with different divergent angles (7.5°, 10.0°, and 12.5°) were tested, showing that larger divergent angles led to shorter distances and times for bubbles to decelerate, increased interaction between gas and liquid, resulting in smaller bubbles, and a lower liquid flow rate needed for bubble breakup. A modified correlation was proposed to predict average bubble size in venturi channels, considering the effect of the divergent angle [16]. The study was further extended by Zhao et al. [18] to investigate the size distributions of bubbles produced by venturi-type generators with different divergent angles (7.5°, 10.0°, and 12.5°) in sewage treatment engineering, where fine bubbles play a crucial role in promoting biochemical reactions. It was found that larger divergent angles or higher liquid flow rates led to the generation of smaller bubbles, accompanied by an increase in number density [17]. Lee et al. [11] investigated the impact of convergent and divergent angles on microbubble size in a venturi nozzle, varying both angles in five values (15°, 22°, 30°, 38°, and 45°), and studied bubble size at each setting through experimental visualisation. The study found that the divergent angle affects the bubble size more significantly than the

***CORRESPONDING AUTHOR | E. A. Alias** | ✉ erny@umpsa.edu.my

convergent angle. The studies indicate that experimental visualisation is a valuable tool for analysing the formation and distribution of bubbles. Nonetheless, it has limitations in measuring detailed or local flow properties in venturi tubes [20]. Alongside experimental visualisation, simulation studies have also proven valuable for examining the complex characteristics of multiphase flows. These simulations provide insights into the detailed flow velocity distribution within venturi channels and the resulting bubble size distribution [12, 21]. Li et al. [19] studied the effects of divergent angles on bubble size through Computational Fluid Dynamics (CFD) simulation. They found that a larger divergent angle leads to smaller bubble size generation due to the presence of high turbulent intensity at the divergent section. Additionally, Lee et al. [11] found that varying convergent and divergent levels affect cavitation. They also discovered, through a computational method, that the mass flow, momentum flux, and effective velocity are affected by the convergent-divergent variations. Willson et al. [12] investigated the effect of divergent angle and throat length-to-throat diameter ratio on the size of the MB produced by a venturi nozzle using CFD simulations. To validate their CFD model, the study compared the computational results with the experimental data they collected. Interestingly, the results revealed that variations in the throat length/throat diameter ratio had only a negligible effect on the generated mean bubble size and size distribution. The combination of experimental and simulation analyses can enhance the accuracy and reliability of results while providing a deeper insight into the relationship between the geometry parameters, flow characteristics, and generated bubble size, in venturi nozzles [14, 15]. Previous studies on Venturi nozzles have primarily focused on flow field characteristics such as pressure drop, velocity distribution, and turbulence intensity using CFD [1]. In contrast, some works have incorporated multiphase modeling to directly predict bubble size distribution (BSD) [12, 21]. Moreover, there is a lack of studies that combine both experimental and simulation methods to analyze bubble size while systematically varying key parameters such as divergent angle and water flow rate [11-13].

Therefore, this study investigates the effects of divergent angle and water flow rate on bubble size generation in a Venturi nozzle through experimental analysis, supported by CFD simulations. A coupled Eulerian–Lagrangian model with a Population Balance Model (PBM) was employed to estimate bubble size and validate experimental results, enabling a direct correlation between flow conditions and bubble size distribution.

2. MATERIAL AND METHODS

2.1 Experimental Visualization

In the experimental visualisation, three venturi nozzles were designed using SOLIDWORK and fabricated via 3D printing. These nozzles featured fixed inlet angles of 19° and divergent angles of 8°, 10°, and 12°, with an air intake at the throat area, as illustrated in Figure 1. The air inlet is crucial for enabling gas entrainment through the pressure drop at the throat, facilitating bubble formation and gas-liquid mixing, which are essential in water treatment and agricultural applications. Experimental visualisation was performed using a high-speed camera (Flowsense EO camera, 2MP, 1600 × 1200 pixels) while varying the water flow rates to 13, 33, and 66 L/min (litres per minute) in a transparent tank (Figure 2). Subsequently, MATLAB software 2016 was utilized for image processing to calculate the mean size of the generated bubbles. Bubble images extracted during the experiments were processed using MATLAB to estimate bubble diameters with precision. Initially, the images were converted to grayscale and contrast adjusted to improve edge visibility. Median filtering was employed to reduce noise and eliminate spurious artefacts. The Sobel filter was then used to detect bubble borders by computing intensity gradients. The processed images were then evaluated using ImageJ, a popular open-source image analysis program. Thresholding was used in ImageJ to generate binary images that could be accurately segmented into individual bubbles. The "Analyze Particles" function was then used to determine bubble size. This tool uses the measured area to calculate the equivalent diameter of each bubble, assuming circular geometry. To ensure accuracy, overlapping or irregular bubbles were eliminated using the aspect ratio and circularity filters. Figure 3 illustrates the outcome of the captured image processed using the Sobel Filter in MATLAB software.

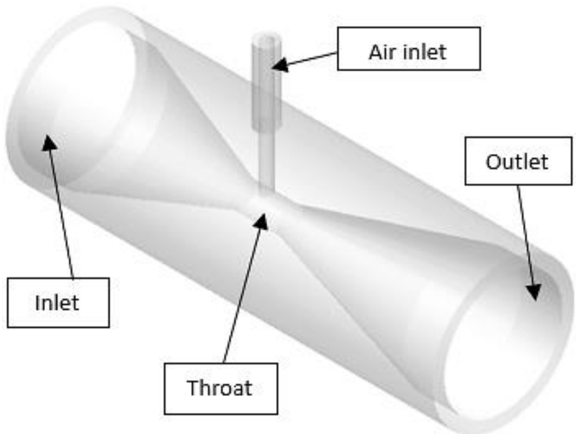

Figure 1. Designed a 3D venturi tube

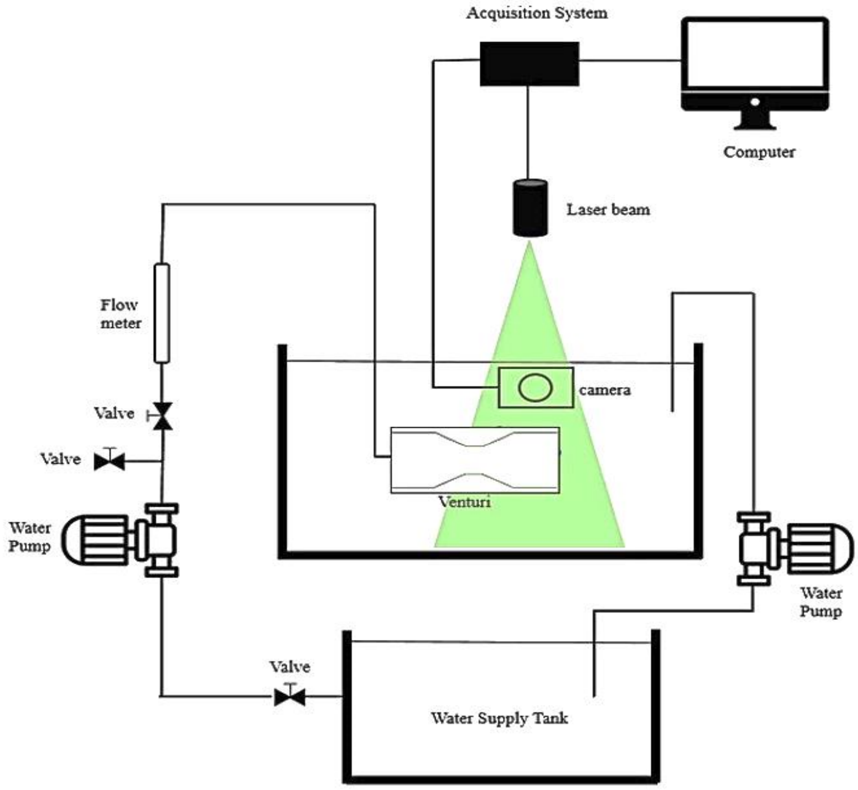

Figure 2. Schematic drawing of experimental setup

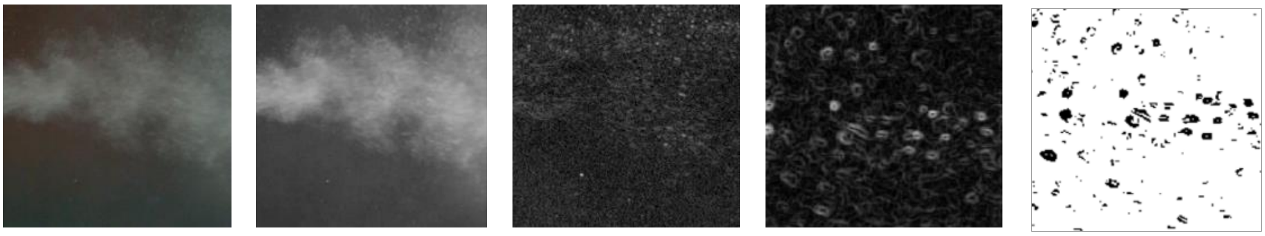

(a) (b) (c) (d) (e)

Figure 3. Image processed through MATLAB software: (a) Raw, (b) Greyscale, (c) Edge detection. (d) Sobel filter cropped and (e) Threshold

2.2 Simulation Analysis

For the simulation analysis, the pressure and flow profiles were resolved in a 2-D axisymmetric domain using ANSYS FLUENT 2021 software. The CFD simulation was conducted using a 2-D axisymmetric domain to reduce computational cost while capturing the dominant flow characteristics in the Venturi nozzle. The geometry used in the experimental visualization was constructed using SolidWorks 2020. Automatic meshing with element sizes ranging from 0.5 mm to 0.1 mm was applied to the overall geometry to determine a suitable element size for the geometry. Additionally, edge sizing with an element size of 0.2 mm was applied at the outlet of the venturi. Figure 4 illustrates the meshing applied through the venturi nozzle. The gas-liquid flow in the venturi channel was investigated using the Eulerian-Lagrangian multiphase and realisable k-ε turbulence model for the solver setup [12, 20-22]. The entrance velocity of water was regulated from 7 to 36 m/s, and the pressure at the output was maintained at one atmosphere. For the air, the pressure is kept at a constant value of 1 atm throughout the experiment. A nonslip boundary condition was chosen as the baseline condition. Liquid water is considered the main phase, and air is composed of a discrete phase.

Table 1 lists the physical parameters of these two fluids. The finite volume approach was used to define the control equations. The velocity–pressure relationship was solved by coupling using the SIMPLE equation. The Population Balance Model was applied to evaluate the bubble size distribution, as described by Ding et al. [21]. The ratio index was set to 2, with a minimum particle size of 0.4 mm and a maximum particle size of 4.33 mm, respectively.

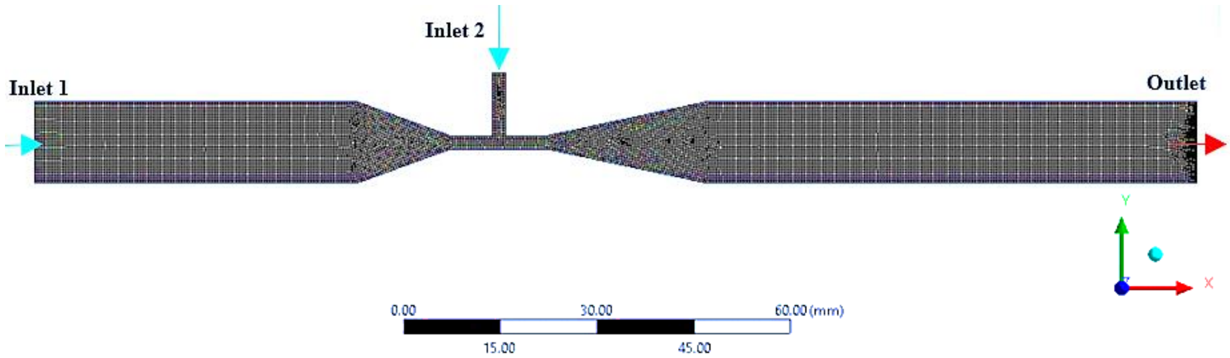

Figure 4. Overall meshing of the venturi

Table 1. Physical properties of water and air

Properties	Water	Air
Density (kg/m³)	997.713	1.188
Viscosity (Ns/m²)	0.001002	0.00001824

2.3 Mesh Independence Test

The mesh independence test was evaluated using a total of five element sizes, ranging from 0.1 mm to 0.5 mm, applied to the geometry accordingly to find suitable meshes for high accuracy in the analysis outcome. The mesh quality analysis shows that element sizes below 0.4 mm achieve mesh convergence for this geometry, as shown in Figure 5. Therefore, for the finalised model, the mesh with an element size of 0.4 mm was determined to be sufficiently precise for the simulation study. This method generated 21,586 nodes and 20,915 elements across the geometry.

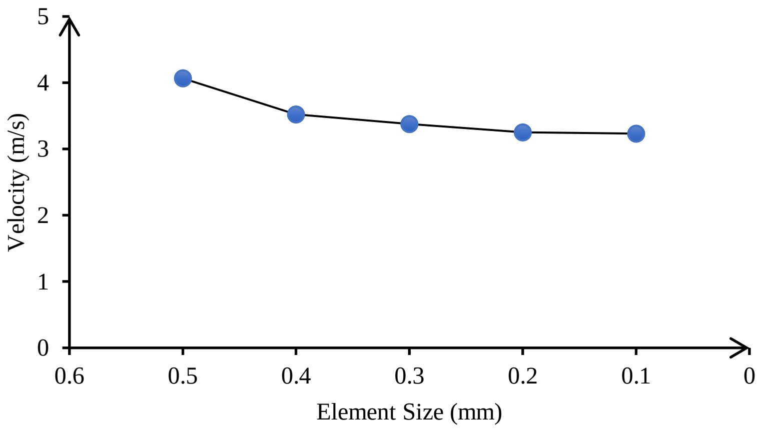

Figure 5. Velocity graph of mesh convergence test

3. RESULTS AND DISCUSSION

3.1 Validation of Experimental Results with Simulation Findings

The validation of simulation results with experimental findings is essential for ensuring the accuracy and reliability of CFD models. Table 2 illustrates the variation in divergent angles used for Venturis 1, 2, and 3. Meanwhile, Table 3 compares the experimental and simulation results for the mean bubble diameter and their relative errors for these three Venturis at a water flow rate of 13 LPM. The relative errors for all venturis are below 5%, indicating a strong agreement between the simulation and experimental data. This agreement demonstrates that the meshing and setup of the simulation are suitable and reliable for analysing the detailed flow characteristics of the venturis.

Table 2. Divergent angle for Venturi 1,2, and 3

Venturi	Divergent Angle
1	8°
2	10°
3	12°

Table 3. Relative error between experimental and simulation of all venturis in 13 LPM flowrate

Venturi	Mean Bubble Diameter (µm)		Relative error calculated (%)
	Experimental	Simulation	
1	1033.494	994.623	3.76
2	786.584	782.158	0.56
3	770.229	739.352	4.00

3.2 Effect of Variation in Divergent Angle and Water Flowrate on Mean Bubble Size

Figure 6 presents a graph of the average bubble diameter generated by all venturis at various divergent angles and water flow rates, obtained through both experimental and simulation analyses. The x and y axes denote the venturi with different divergent angles and bubble diameters in µm, respectively. The results show that the generated bubble sizes range from 505 µm to 1033 µm for both the experimental and simulation outcomes.

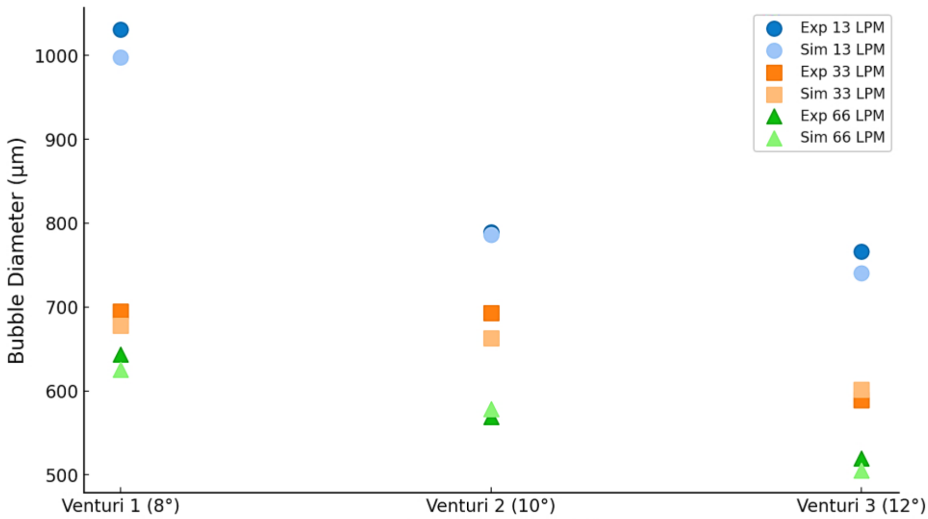

Figure 6. Average bubble size with different divergent angles and water flow rates

In terms of variation in the divergent angle, Venturi 3, with a 12º angle, reported smaller bubble formation compared to Venturi 1 and 2. The smallest bubble generated by Venturi 3 in the experiment was 519 µm, while in the simulation, it was 505 µm at a water flow rate of 66 L/min. The simulation results closely match the experimental findings, with a maximum relative error of 4.00%, indicating a strong agreement between the two sets of data. Zhao et al. [10] found that a wider outlet angle results in a shorter residence period, which in turn enhances the liquid-gas interaction and promotes bubble breakup [12, 22]. As the divergent angle increased, the diameter of the bubble decreased. This trend suggests that a larger divergent angle produces smaller bubbles, whereas a smaller angle yields larger bubbles. The relationship between water flow rate and bubble size in the produced MBs is strong, with a lower water flow rate resulting in larger bubbles, even at larger outlet angles [22]. As demonstrated in Figure 3, the bubbles formed in Venturi 3 were smaller than those in Venturi 1 and 2. However, a significant difference in bubble size was still observed in Venturi 3 due to variations in water flow rate, with 66 L/min producing the smallest bubbles compared to 13 and 33 L/min. These findings align with previous studies that have shown an inverse relationship between water flow rate and bubble size [13, 16, 23–27]. Furthermore, under all conditions, the mean size of the MBs decreases as the water flow rate increases. This trend is attributed to the bubble having less time to encounter the gas flow channel, thereby overcoming the inertial force caused by surface tension [27].

Figure 7 illustrates the influence of variations in the divergent angle on the flow velocity in the venturis. Generally, owing to the presence of constriction at the throat section of the venturi, there will be a significant rise in the velocity in this section compared to the convergent and divergent sections of the venturi [12]. Sudden changes in geometry lead to substantial alterations in flow properties, including pressure and turbulence intensity. The same pattern can be observed in all venturis in this study, where the velocity increases at the throat section due to a reduction in the area. The variation in the divergent angle influences the drop in flow velocity in the divergent section. The maximum velocity occurs when the bubble experiences a larger flow resistance at a larger divergent angle [28]. All three angles (θ = 8.0°, 10°, and 12°) yielded average flow velocities of approximately 3.24, 5.27, and 7.89 m/s, respectively, at a water flow rate of 13 L/min. Overall, the comparison between different divergent angles shows that the greater the divergent angle (Venturi 3), the higher the velocity, and this reduces the time and distance needed for the bubble to descend. This also implies that inducing a lower motion of bubbles in the diverging part is important for establishing better contact between the gas and liquid, which is advantageous for collapsing into tiny bubbles [28].

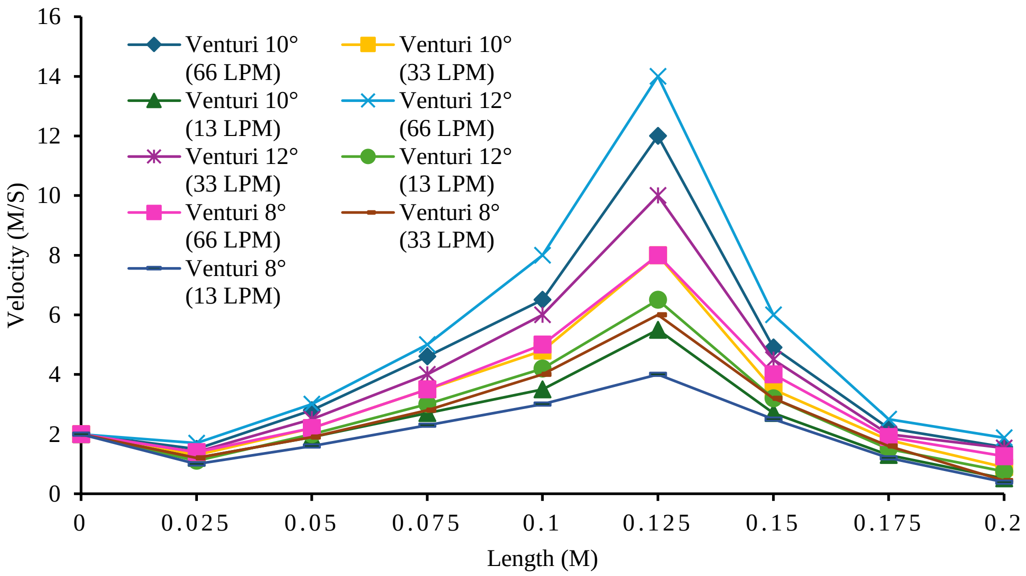

Figure 7. Effect of different divergent angles and water flowrate on flow velocity in venturis

The variation in flow rate in Figure 6, which ranged from 13 L/min to 33 L/min and 66 L/min, also influenced the mean bubble velocity at various water flow rates for Venturi 1. Venturi at 66 LPM illustrates the huge velocity drop at the divergent section. This will induce cavitation to occur. Firstly, higher water velocities can create stronger suction forces, drawing in more air and potentially increasing the number of bubbles formed. Secondly, increased water flow rates can alter the flow patterns within the venturi, affecting the distribution and size of the bubbles produced. Finally, higher velocities can also influence the residence time of water within the venturi [29], potentially impacting the rate and efficiency of bubble formation. Table 4 presents the summarised results for both different divergent angles and water flow rates accordingly. Overall, the relationship between water flow rate, velocity, and bubble generation in a Venturi is complex and may vary depending on other factors, such as Venturi geometry and flow conditions [12, 17, 18].

The use of CFD to predict bubble size, validated against experimental data, highlights the suitability of divergent angle and water flow rate as tuning parameters. These parameters directly modulate velocity gradients, which induce shear stress in the divergent region, which are the primary drivers of bubble breakup, as confirmed by simulation.

Table 4. Summarised results for the effect of different divergent angles and water flowrate

Venturi	Divergent Angle	Water Flow Rate	Average Bubble Diameter (Exp.)	Average Bubble Diameter (Sim.)	Impact of Divergent Angle and Water Flow Rate
Venturi 1	8º	13 LPM	1033 µm	995 µm	Smaller angle → Larger bubbles Larger angle → Smaller bubbles
		33 LPM	787 µm	782 µm	
		66 LPM	770 µm	739 µm	
Venturi 2	10º	13 LPM	694 µm	678 µm	Lower flow rate → Larger bubbles Higher flow rate → Smaller bubbles
		33 LPM	693 µm	662 µm	
		66 LPM	589 µm	601 µm	
Venturi 3	12º	13 LPM	643 µm	625 µm	
		33 LPM	569 µm	578 µm	
		66 LPM	519 µm	505 µm	

3.3 Cavitation and Bubble Formation

Although cavitation was not the primary focus of this research, its significance in bubble generation in Venturi nozzles cannot be neglected. As shown in Figure 8, a rapid increase in flow through the throat can result in a significant pressure decrease, which could lead to cavitation when the pressure drops below the vapour pressure of water. This could trigger the occurrence of vapor cavities or bubbles, which can expand or collapse depending on the recovery pressure in the diverging section. The observed velocity peak in the throat region and subsequent expansion downstream qualitatively support the possibility of cavitation, particularly at higher flow rates and bigger divergent angles [21-25].

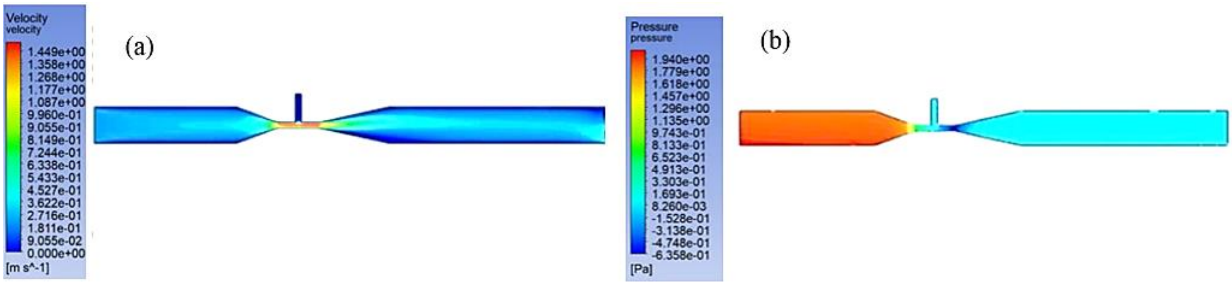

Figure 8. Venturi 1 at 13 LPM: (a) velocity and (b) pressure contour

At the highest tested flow rate of 66 LPM, Venturi 3 (12°) produced the smallest bubble, measuring 505 µm in simulation and 519 µm experimentally (Figure 6). These conditions also showed the highest velocity gradients of 14.09 m/s (Figure 7), which, according to Bernoulli's principle, would correspond to the lowest static pressures and further support the possibility of cavitation-induced bubble breakup. Although our CFD model did not explicitly incorporate a cavitation model, the velocity profiles and flow behaviour under high-flow, wide-angle conditions are consistent with those found in cavitation-prone environments. This suggests that cavitation may contribute to the enhanced bubble fragmentation observed, and future studies should include cavitation modeling to verify this mechanism more precisely.

To better understand their direct contribution to bubble size under various Venturi geometries and flow rates, future work will expand this analysis by incorporating cavitation-specific models, such as the Schnerr–Sauer or Zwart–Gerber–Belamri models. This will enable the quantification of vapour volume fractions and cavitation intensity. Moreover, this study employed a 2-D axisymmetric CFD model to simulate flow and bubble dynamics in the Venturi nozzle. While this approach effectively reduces computational cost and provides meaningful insight into the flow structure and bubble size distribution trends, it inherently simplifies the actual three-dimensional nature of the flow. As a result, complicated processes such as asymmetric vortex generation, secondary flow structures, and fluctuations in local turbulence strength may not be adequately represented. Furthermore, cavitation was discussed through the interpretation of velocity fields rather than direct simulation with cavitation models, which limits our ability to quantify vapor formation and collapse processes. Finally, while the Eulerian-Lagrangian model's calculation of bubble size agreed well with experimental results, uncertainties remained due to assumptions in drag force modelling and particle-fluid interactions. Future research should address these limitations by utilising full 3D simulations and sophisticated cavitation models to enhance prediction accuracy.

4. CONCLUSIONS

In this study, experimental and computational methods are employed to investigate the impact of divergent angles and water flow rates on bubble size. An experimental visualisation study utilised a high-speed camera to measure bubble size, while ANSYS FLUENT simulations provided detailed bubble size and flow characteristics. Overall, the comparison of the MB sizes in the simulation study and experimental visualisation shows a relative error of less than 5% for all venturis, which complies with the inclusion of a simulation study that validates and complements the shortcomings of the results obtained via experimental visualisation. Simulation studies also provide extended flow characteristic outcomes, such as the flow velocity distribution in the venturis. In terms of geometry and flow parameters, the divergent angle and water flow rate play significant roles in determining the bubble size in the venturi generator; the bubble diameter decreases as the divergent angle and water flow rate increase. According to these observations, the MB breakup phenomenon may be influenced by larger flow rates and divergent angles. Meanwhile, the venturi with a 12º divergent angle and 66 LPM water flow rate produced the smallest bubble diameter, which ranged from 505 to 519 µm. Hence, a combination of both experimental and computational analyses will yield higher-quality results compared to a single analysis (experimental or computational) alone.

ACKNOWLEDGEMENTS

The authors are grateful to the Ministry of Higher Education Malaysia and Universiti Malaysia Pahang, as well as Al-Sultan Abdullah (www.umpsa.edu.my), for the financial support provided under FRGS/1/2022/TK08/UMP/02/26 (University Reference No. RDU220115) and RDU220339. The authors would also like to express gratitude to the Centre for Research in Advanced Fluids, Universiti Malaysia Pahang, and Al-Sultan Abdullah for the insight and expertise that greatly assisted the present research work.

CONFLICT OF INTEREST

The authors declare that they have no conflicts of interest.

AUTHORS CONTRIBUTION

N. Nadumaran (Formal analysis; Visualisation; Writing – Original Draft)

E. A. Alias (Conceptualisation; Validation, Writing – review & editing; Funding acquisition; Resources; Supervision)
M. H. Hamidi (Data curation; Visualization)
N. H. Johari (Review; Supervision)

AVAILABILITY OF DATA AND MATERIALS

The data is available upon request.

ETHICS STATEMENT

Not applicable

REFERENCES

[1] V. Balasubramanian, K. Adalarasu, R. Regulapati, "Comparing dynamic and stationary standing postures in an assembly task," *International Journal of Industrial Ergonomics*, vol. 39, no. 5, pp. 649–654, 2009.

[2] N. M. Ali, F. Dzaharudin, E. A. Alias, "Nonlinear dynamics of a shell encapsulated microbubble near solid boundary in an ultrasonic field," *Journal of Mechanical Engineering and Sciences*, vol. 14, pp. 7235–7243, 2020.

[3] A. Erny, D. Fatimah, I. Muhammad, "Fundamental characteristics of microbubbles in water and diesel fuel," in *Proceedings of the MATEC Web of Conferences: International Conference on Advanced Technology and Applied Sciences (ICaTAS 2018)*, vol. 225, pp. 1–6, 2018.

[4] E. A. Alias, "Skin friction reduction by micro bubbles in pipe flow," *Master Thesis*, Tokai University, Japan, 2016.

[5] Q. Li, C. Zhang, L. Yang, Y. Chen, Z. Wang, Z. Yin, "Hydrodynamic cavitation: A promising technology for industrial-scale synthesis of nanomaterials," *Frontiers in Chemistry*, vol. 1, pp. 259–271, 2020.

[6] H. H. Sang, X. Y. Jiao, S. F. Wang, W. H. Guo, M. K. Salahou, K. H. Liu, "Effects of micro-nano bubble aerated irrigation and nitrogen fertilizer level on tillering, nitrogen uptake and utilization of early rice," *Plant, Soil and Environment*, vol. 64, no. 7, pp. 297–302, 2018.

[7] K. C. S. Liew, H. H. Lau, C. W. Oon, R. R. Praveena, M. H. Ng, H. L. Lam, "Porous venturi-orifice microbubble generator for oxygen dissolution in water," *Processes*, vol. 8, no. 10, pp. 1–15, 2020.

[8] J. Hanotu, H. C. H. Bandulasena, W. B. Zimmerman, "Aerator design for microbubble generation," *Chemical Engineering Research and Design*, vol. 123, pp. 367–376, 2017.

[9] P. Arumugam, "Understanding the fundamental mechanisms of a dynamic micro-bubble generator for water processing and cleaning applications," *Master Thesis*, Engineering University of Toronto, Canada, 2015.

[10] W. Budhijanto, D. Darlianto, Y. S. Pradana, M. Hartono, "Application of micro bubble generator as low cost and high efficient aerator for sustainable fresh water fish farming," in *Proceedings of the AIP Conference: International Conference on Green Energy and Applications*, vol. 1840, pp. 1–6, 2017.

[11] C. H. Lee, H. Choi, D. W. Jerng, D. E. Kim, S. Wongwises, H. S. Ahn, "Experimental investigation of microbubble generation in the venturi nozzle," *International Journal of Heat and Mass Transfer*, vol. 136, pp. 1127–1138, 2019.

[12] D. A. Wilson, K. Pun, P. B. Ganesan, F. Hamad, "Geometrical optimization of a venturi-type microbubble generator using CFD simulation and experimental measurements," *Designs*, vol. 5, no. 1, pp. 1–18, 2021.

[13] L. Zhao, L. Sun, Z. Mo, J. Tang, L. Hu, J. Bao, "Effects of the divergent angle on bubble transportation in a rectangular Venturi channel and its performance in producing fine bubbles," *International Journal of Multiphase Flow*, vol. 114, pp. 192–206, 2019.

[14] A. Gordiychuk, M. Svanera, S. Benini, P. Poesio, "Size distribution and Sauter mean diameter of microbubbles for a Venturi type bubble generator," *Experimental Thermal and Fluid Science*, vol. 70, pp. 51–60, 2016.

[15] A. Fujiwara, K. Okamoto, K. Hashiguchi, J. Peixinho, S. Takagi, Y. Matsumoto, "Bubble breakup phenomena in a Venturi tube," in *Proceedings of the 5th Joint ASME/JSME Fluids Engineering Summer Conference (FEDSM2007)*, vol. 1, pp. 553–560, 2007.

[16] X. Wang, Y. Zhang, L. Wang, C. Liu, Q. Feng, J. Huang, "Bubble breakup in a swirl-venturi microbubble generator," *Chemical Engineering Journal*, vol. 403, pp. 126397–126410, 2020.

[17] L. Zhao, L. Sun, Z. Mo, J. Tang, L. Hu, J. Bao, "A visualized study of the motion of individual bubbles in a venturi-type bubble generator," *Progress in Nuclear Energy*, vol. 97, pp. 74–89, 2017.

[18] L. Zhao, L. Sun, Z. Mo, J. Tang, L. Hu, J. Bao, "An investigation on bubble motion in liquid flowing through a rectangular Venturi channel," *Experimental Thermal and Fluid Science*, vol. 97, pp. 48–58, 2018.

[19] J. Huang, L. Sun, Z. Mo, Y. Feng, J. Bao, J. Tang, "Experimental investigation on the effect of throat size on bubble transportation and breakup in small Venturi channels," *International Journal of Multiphase Flow*, vol. 142, pp. 103737–103752, 2021.

[20] K. Sakamatapan, M. Mesgarpour, O. Mahian, H. S. Ahn, S. Wongwises, "Experimental investigation of the microbubble generation using a venturi-type bubble generator," *Case Studies in Thermal Engineering*, vol. 27, pp. 101238–101251, 2021.

[21] M. Li, A. Bussonnière, M. Bronson, Z. Xu, Q. Liu, "Study of Venturi tube geometry on the hydrodynamic cavitation for the generation of microbubbles," *Minerals Engineering*, vol. 132, pp. 268–274, 2019.

[22] G. Ding, J. Chen, Z. Li, X. Cai, Y. Ji, "An investigation on the bubbly flow of a Venturi channel based on the population balance model," *Canadian Journal of Chemical Engineering*, vol. 100, no. 7, pp. 1652–1664, 2022.

[23] N. Niellambare, H. H. Mohamad, A. A. Erny, H. J. Nasrul, "Investigation on the effect of Venturi geometry variation on microbubble generation," in *Proceedings of the AIP Conference: 3rd International Conference on Mechanical Engineering Research (ICMER 2022)*, vol. 2610, pp. 1–8, 2022.

[24] M. Sadatomi, A. Kawahara, K. Kano, A. Ohtomo, "Performance of a new micro-bubble generator with a spherical body in a flowing water tube," *Experimental Thermal and Fluid Science*, vol. 29, no. 5, pp. 615–623, 2005.

[25] N. Suwartha, D. Syamzida, C. R. Priadi, S. S. Moersidik, F. Ali, "Effect of size variation on microbubble mass transfer coefficient in flotation and aeration processes," *Heliyon*, vol. 6, no. 4, pp. e03748–e03760, 2020.

[26] S. Y. Jeon, J. Y. Yoon, C. M. Jang, "Bubble size and bubble concentration of a microbubble pump to operating conditions," *Energies*, vol. 11, no. 7, pp. 1–14, 2018.

[27] C. A. Sennoga, E. Kanbar, A. Bouakaz, "An ImageJ plugin for the sizing and counting of microbubbles," in *Proceedings of the IEEE International Ultrasonics Symposium (IUS 2015)*, pp. 1–4, 2015.

[28] J. Huang, L. Sun, Z. Mo, J. Tang, L. Hu, J. Bao, "An investigation on the performance of a micro-scale Venturi bubble generator," *Chemical Engineering Journal*, vol. 386, pp. 120980–120995, 2020.

[29] L. Sun, Z. Mo, J. Tang, L. Hu, J. Bao, Y. Feng, "Characteristics and mechanism of bubble breakup in a bubble generator developed for a small TMSR," *Annals of Nuclear Energy*, vol. 109, pp. 69–81, 2017.